

AUTOMATIC MOSAICING OF SATELLITE IMAGES USING GLOBAL RE-NAVIGATION

A. Mandanayake, A. Newton, K. Tildsley and J-P. Muller
Department of Photogrammetry and Surveying,
University College London,
Gower Street,
London WC1E 6BT,
UK
INTERNET:athula@ps.ucl.ac.uk

ABSTRACT

An automated satellite multi-image registration and mosaicing system based on automatic tie-point extraction and re-navigation has been developed for AVHRR, TM, Viking Orbiter and pre-geocoded images. The geometric aspects of image to image and image to ground registration form the core of any such work. However a significant amount of pre-processing and some post-processing is needed to produce seamless mosaic, in particular for AVHRR and LANDSAT-TM. Results for AVHRR multi-scene registration in the Rondonia area of Brazil, Aral Sea, and LANDSAT-TM SOM of Kuwait are presented. Initial estimates of accuracy show RMS inter-scene registration of 0.4 km (0.36 pixels) for two resampled AVHRR scenes in Rondonia, 0.5 km (0.45 pixels) for five AVHRR scenes in Aral Sea and 9.5m (0.33 pixels) for two LANDSAT-TM SOM scenes in Kuwait. Analysis of the effect of the scan angle on tie-point and inter-image registration accuracy are included. A seamless mosaic of LANDSAT-TM SOM scenes in Kuwait is also presented.

KEY WORDS: Automatic Tie-Pointing, Global Re-navigation, Automated Registration, AVHRR and LANDSAT-TM mosaics.

1. INTRODUCTION

This paper describes the current status of the UCL MOSAIC (Mosaicing of Satellite Images using Automated Image Correlation) system (Muller et al 1992[14], Newton et al 1992[19]) based on automatic tie pointing and re-navigation developed at UCL. The system can mosaic AVHRR, LANDSAT-TM, Viking Orbiter and pre-geocoded images. Mosaicing of Viking Orbiter imagery and its accuracy is discussed in Muller et al (1992)[16]. The key points of UCL MOSAIC are: (1) Automatic preprocessing of the input data. (2) Automatic selection of corresponding tie points using a patch based matcher. (3) Global re-navigation via a mathematical optimisation method which minimises the total geometric error in the mosaic. (4) Resampling to output space. The central advance of the UCL MOSAIC system is in the area of automatic tie point generation. This builds on work already carried out at UCL on general automatic seed point and tie-point generation. Allison et al (1991)[2](Allison and Muller 1992[1]) demonstrated generation of such points for SPOT stereo pairs, digitised aerial photography and airborne scanner (ATM and ASAS) imagery. During the entire mosaicing process, images, labels, error logs and tabular data are used to manipulate and keep track of the variables and complex operations required to construct a mosaic. The system is currently implemented on UNIX based workstations. The mosaicing philosophy is based on the Jet Propulsion Laboratory's planetary image mosaicing system (Barragy and Evans[4]). AVHRR preprocessing is based on the APOLLO system developed by the UK Meteorological Office (Saunders and Pescod 1988[24]).

The immediate aim of the AVHRR work has been to allow a large number of views of an area to be registered together for studies of temporal change and subsequently for composite image sequences to be used in the visualisation of the change process (Muller and Schreier 1992[15]). The work with TM data was also primarily for visualisation purposes - to create a mosaic of the whole of Northern Germany (Newton et al 1992[19]) for use in an animation of the effects of sea level rise. The work forms part of a long-term project to build global land cover mapping products using automated image understanding techniques (Muller 1989[12]).

The basic scheme is centred on the creation of a set of pixel to pixel correspondences between image points, or tie-points, analogous to the pixel to point correspondence of ground control points (GCPs) in geocoding. Such points are then used through an image to image or image to ground transformation to co-locate images in the output mosaic space.

For image map creation over large multi-pass areas, across image boundaries, over areas seldom imaged clearly (because of cloud or atmospheric effects), where GCPs are inaccurate, sparse or not available, or for routine regeneration of such data, automation of the tie-pointing process represents significant saving in time and effort. Indeed in many cases it may result in an improved product in comparison to human operator-based tie-pointing or GCP selection.

Finally there is a scientific imperative for such automated registration of multiple scene views - for change detection, multi-look viewing (eg. for NDVI compositing, vis Holben 1986[10]), and for multi-directional viewing of targets, (e.g. for BRDF for albedo studies Barnsley and Muller 1991[3]) if global monitoring is to be performed.

2. MOSAICING PROCEDURE AND IMPLEMENTATION

The mosaicing process can be broken down into a number of logical steps: pre-processing, selection of tie points, re-navigation, resampling to output space and compositing and mosaicing with radiometric blending. The mosaicing process and implementation are briefly described at this point for AVHRR imagery. More details of this can be found in Newton et al 1992[19]. Automated image preprocessing and re-navigation are highly mosaic/mission dependent but the mechanism of tie point generation and resampling are common to all input image types. Potential tie-points are found on a pairwise basis even where a particular region may be contained within more than two of the input scenes. The very large areas covered by AVHRR scenes and their moderate resolution imply that AVHRR mosaics are regional, country or continental in scale. However often it is extremely difficult, or impossible, to find a single AVHRR scene which is cloud free over the whole area of interest. Hence it is necessary to combine multiple views of the area to achieve the required total cloud-free coverage. Figure 1 shows a schematic diagram of the AVHRR processing system.

2.1 Pre Processing

All of the AVHRR data pre-processing that has been used for this work is based on the "APOLLO" ("AVHRR Processing Over Land Cloud and Ocean") system developed for the UK Meteorological Office at the Clarendon Laboratory in Oxford, UK (Saunders and Pescod 1988[24]) but has been ported to Unix from its original VAX/VMS implementation. Pre-processing consists of the detection of clouds and the computation of approximate navigation prior to tie-point generation. During navigation correction the AVHRR camera-

model parameters are adjusted to optimise ground location. Subsequently corrections for gross solar zenith angle illumination variation effects and atmospheric effects need to be applied to make the composited images more radiometrically consistent.

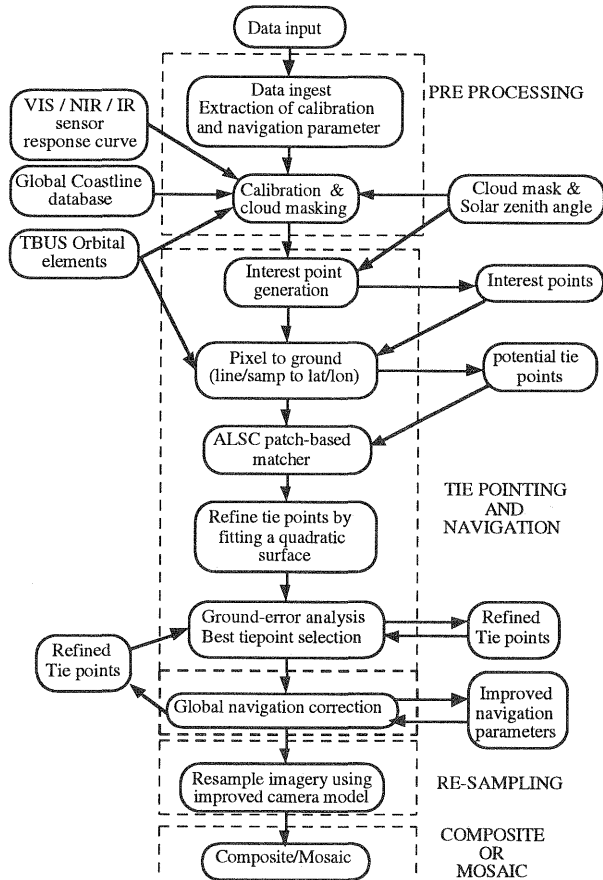


Figure 1. Schematic of the complete process for AVHRR imagery

2.1.1 Cloud detection

Cloud detection and masking is essential prior to interest point generation because of the potential of high contrast edges of the clouds to be misidentified as potential tie points. Hence unless masked out prior to the interest point generation stage a very large number of points not related to the texture of the underlying surface will go forward to the correlation process. Ideally as transient points not present in the other scenes these would fail the tie-point selection tests. However if there are a significant number of cloud related points that pass the initial correlation test they risk contaminating the subsequent screening processes that rely on the tie-point set being correct.

Existing cloud detection schemes can be subdivided into the physical model based algorithms, such as those in APOLLO (Saunders 1988, 1990[23][22][21]), and those seeking to divide images into classes of pixels before assigning types, e.g. land, sea, cloud (snow,ice,etc.), to the classes so found on the basis of similar physical rules (Gallaudet 1991[8] and Simpson 1990[25]). Unfortunately all such rules are necessarily based on finding, for the different bands of the imagery or for the differences between a pair of bands, empirical thresholds to delineate cloud from cloud contaminated and from cloud-free pixels. All of the APOLLO tests, and their built-in defaults, have been, for historical reasons, optimised for the UK and Western Europe. Here these have been applied over the Aral Sea and Rondonia areas and this has required certain tests to be dropped. Unfortunately space does not permit a detailed discussion of these issues here.

A further problem is cloud shadow. This is more detrimental to the final mosaic when included in the input images to the

mosaicing process than in the tie-pointing process. Currently no direct solution to this problem is used. Instead, for the purposes of cloud masking cloud shadow is removed by expanding the cloud mask regions using morphological operators.

3 TIE POINT GENERATION

This process can be broken down into a number of steps: finding interest points, pairing them between overlapping images to generate potential tie point conjugates, correlation by an area based matcher around the tie point conjugates and tie point culling. Considering now all pairs of overlapping input images an attempt is made to find, on a pairwise basis, a correlation between interest points in the two images. To aid this description the terminology of stereoscopic viewing is adopted to refer to the two images as the 'left' and 'right' view. Of course it is not necessary for them to be actually left or right looking views - but as the correlation process is not completely symmetric between the two images this terminology is useful. At the centre of tie point generation is the use of the Adaptive Least Squares Correlation (ALSC) algorithm (Gruen (1985)[9]) as implemented at UCL as part of the Alvey MMI - 137 project Otto and Chau (1989[20]) which attempts to correlate a region around a left-image interest point with the image patches surrounding a number of, tie-point candidate, right-image interest points.

3.1 Interest Point Generation

The Foerstner (1986[6], 1987[7]) operator is employed to find "interesting" points in each input image. It has been adapted to employ an exclusion mask, for our purposes the image cloud and sea mask, within which area no interest points are found. This is used to exclude cloud contaminated regions from the interest point generation. If the operator is employed over a substantial window (5 pixels across) it returns points which may be suitable for correlation by an area based matcher, such as the Adaptive Least Squares Correlation (ALSC) algorithm (Gruen (1985)[9]) operator. Thus these two operators, in series, form the basis of a multi-point correlation scheme. It is important, for all applications of tie-pointing, that no positional bias is present in the final set of utilised tie-points. Interest points which go forward to the inter-point correlation process are selected by thresholding their Foerstner operator value. Alternatively a count threshold can be employed and the 'N' most interesting points retained. If applied over the entire image, without other constraints, the resulting distribution of points was found to be generally unsatisfactory. It is apparent that different thresholds need to be applied to different regions of the image. Thus the images are 'tiled' and the N/k (k tiles in the image) most interesting points in each tile selected. Sub-pixel location (Foerstner 1987[7]) is achieved by taking the weighted centre of "gravity" of the Foerstner operator window.

3.2 Disparity Limitation

Input images are usually accompanied by ancillary data on their nominal location, (for pre-geocoded images) or on the sensor's position and orientation during image acquisition (for images still in satellite relative form, e.g. AVHRR or LANDSAT-TM Space Oblique Mercator hereafter referred to as "raw" images). This allows the potential location of a left-image point in the right image space to be restricted. Again using stereo terminology, the difference between a point's left image coordinates and its right image coordinates, as a 'distance', is termed its disparity. Permitting tie point pairs below a certain disparity threshold results in the required short-list of candidate right-image points for subsequent correlation. For raw images this operation is performed in mosaic output coordinates.

3.3 ALSC patch correlation

Correlation is attempted, for each left image point, with each of its potential right image points in turn. Where the iteration process fails to converge no correlation will be found. Thus such interest-point pairs are rejected.

The most commonly used measure of the success of the correlation is the eigenvalue of the variance and covariance matrix. This eigenvalue is not an unbiased estimate of the 'quality' of inter-patch correlation - its value is effected by the mean grey-level within the patches. This means that it is difficult to set a fixed eigenvalue threshold for all types of imagery and all scenes and treat matches with lower eigenvalues as uniformly correct and others as errors. However it can be used to choose, from a set of matches to a single left image point, the best match and hence the most likely tie-point pair. At this stage there exists, for each overlapping pair of input images, a set of tie-points a large majority of which should be correct. The relative positions of all the images are adjusted so as to minimise the residual distances between tie-points in the output space. However the convergence process has been shown to be sensitive to the remaining erroneous points in the tie-point set so their prior removal is a necessity to reach convergence.

3.4 Tie-point Culling

A number of further checks on tie-point validity can be performed - either through knowledge of the imaging geometry or by looking for local consistency between tie-points without employing knowledge of the sensor. It is important to avoid applying constraints which will lead to the rejection of good points, particularly where they do not allow for the geometric extremes of the data, as this may lead to rejection of points in particular areas of the image, e.g. at the swath edge (which is useful for BRDF studies), and hence a positional bias in the final tie-point set. However these points are likely to be poor in resolution so weights still need to be attached.

In Allison et al (1991[2]) an example is given of fitting a polynomial surface to the tie-point set as a Least Squares fit. In this process the left and right image tie-point coordinates are matched to a quadratic surface (as if used as tie-points to find a quadratic warp from the left to right image space). For each point a residual difference between the computed surface and the original results is computed. Where this residual falls more than a threshold number (one) of standard deviations (SD) away from the surface the corresponding tie-point is rejected. The process is repeated until the overall SD is less than a set threshold (2.5) value. For a vary wide swath instrument, e.g. AVHRR, the curvature of the Earth's surface introduces image distortions which means that a polynomial warp cannot be used to map from image to ground space. For mappings between a pair of AVHRR images this translates to tie-points which cannot be modelled by a polynomial surface. In practise it has been found that the quadratic surface check can still be used where the images have a near common sub-satellite track.

A new check was introduced, for raw imagery, which examines the distribution of tie-point differences as vectors in ground coordinates after transformation of images to ground from the orbital model. The orientation and magnitude of these vectors are analysed statistically. Vectors whose magnitude or orientation are beyond one standard deviation from the mean of this population are rejected.

4 GLOBAL RE-NAVIGATION FOR RAW IMAGES

Using the initial navigation (camera parameters from raw data) as a first estimate the ground position (lat, lon) of each tie point can be computed. From these positions the ground inter-point distance or the residual distance in the point's ground coordinates is computed. Summing all of these residual differences in the point's ground coordinate yields a value for the total geometric error or the inconsistency between frames. The camera pointing and the position of the satellite location vector is altered until the error is minimised. Total error is defined to be the square root of the mean weighted sum of the squared residual distances. Using these weights, certain tie-points can be emphasised over others. This is very useful for emphasising ground control points or near nadir points in AVHRR. During the mosaicing process described here all points are given one unit weight. Adjusting the parameters of both the scenes in which the tie-point has been located to

minimise the mismatch distance in the point's ground coordinates should result in good registration of the two scenes in the vicinity of that point. Adjusting all the scene's camera parameters simultaneously to minimise the total mismatch distance for all points across all image pairs should result in the optimal final imaging parameter values for the entire mosaic. This is based on the block triangulation adjustment principle (Slama 1980[26]). A conjugate gradient procedure is used to achieve the minimisation.

An important proviso of this technique, for image mapping as opposed to inter-image registration, is that the result of navigation convergence is a relative, rather than an absolute, correction of image to ground coordinates. Clearly an absolute correction still requires the use of some form of ground control points (GCPs). However if the errors in initial navigation are not systematically biased then the converged solution can be expected to be, overall, more accurate than the initial navigation. The prospect exists, with this technique, of performing GCP selection and location once, for a particular area, and then using automatic tie-pointing between this located scene and a new scene to locate the new scene without renewed GCP selection. An example data set global image mosaic developed for this purpose is described in Muller et al (1992)[17]. Another complication is the effect of topography on tie-point location. Muller and Eales 1990[13] have analysed coarse global topography datasets to quantify this geometric effect for AVHRR and the EOS project MODIS sensors. Their work suggests that GCP ought to be avoided in areas of variable relief.

4.1 Position Correction for Pre-Geocoded Images

The other class of images processed is that which has been pre-geocoded. This process is only used where significant residual errors make position correction by tie-pointing necessary. This is often the case even where relatively good GCPs have been employed. Systematic inconsistencies, potentially introduced by using multiple maps from different sources or at different scales, can be reduced, or removed, by shifting the input images relative to their nominal location.

5 RESAMPLING

Having converged the navigation for mosaic input scenes to a mutually consistent set of geometric parameters they can be resampled using the camera model employed for convergence. The resampling used is piecewise bilinear interpolation and can be described as: (1) transformation of a regular input grid to ground coordinates and to mosaic space, (2) bilinear interpolation of coordinates and DN values. This method is used because calculating the full mapping for each pixel is too time consuming. For AVHRR imagery the input image pixel scan angle is also calculated and written as a floating point array in the mosaic output space. This can be used to select the best (highest resolution) input pixel for each output pixel if more than one input image covers that pixel, or to calculate weights for each input pixel if the output is a composite.

6 MOSAICING OR COMPOSITING AND IMAGE BLENDING

Images are mosaiced or composited depending on the location, mission and application. For example if we are studying land surface change over time (eg. deforestation in Rondonia, water body shrinkage of the Aral Sea) mosaicing is the preferred option. In the mosaicing process input image boundaries may be visible in the output as seam lines. This effect can be caused by misregistration, changes in the atmospheric transmittance, reflectance or BRDF effects, illumination effects of sun angle, seasonal changes of the surface reflectance, precipitation, and changes caused by human activities. Improvements to the mosaicing of TM images are achieved by changing the grey levels of the images to match the average brightness in the overlapping area. This method has been applied to TM-SOM data of Kuwait and pre-geocoded TM data of North Germany. However this is not sufficient to eliminate completely the seam artefacts. Additional radiometric blending is applied to reduce the visible impact of the seams. Blending is done by changing

the grey level of the overlapping region as :

$$G(x,y) = g_1(x,y) + (g_2 - g_1)(D-d)/D \quad (1)$$

where g_1 and g_2 are grey-levels of two overlapping images, (x,y) a point in the overlapping region, d the shortest distance to the edge, D is a pre-defined constant (blending distance).

Another method tested was a linear transformation of grey levels in the overlapping area (Barragy 1988[4]). This gave large areas of saturation due to clouds, haze and smoke in those images and was deemed unsuitable for any visualisation purposes.

At the compositing/mosaicing stage the user has a choice of six different methods:

- (1) compositing by using maximum normalised difference vegetation index (NDVI)(Holben 1986[10]).
- (2) compositing by using NDVI weighted by scan angle.
- (3) averaging all pixels in the overlap areas.
- (4) averaging all pixels in the overlap areas with scan angle weighting.
- (5) mosaicing.
- (6) mosaicing images with a no data value .

The first two methods only are used for AVHRR mosaicing. Normalised difference vegetation index (NDVI) (Kidwell 1990[11]) is calculated as:

$$NDVI = (NIR - VIS)/(VIS + NIR) \quad (2)$$

where NIS - visible (<670nm) channel 1 DN value and NIR channel 2 (0.7-1µm) DN value.

Full range (-1, 1) of the NDVI is used when selecting the best cloud free pixel. The weighted NDVI is calculated by dividing NDVI by the relative size (size of a pixel over nadir is unit) of the input pixel to cater for the geometric effect of the scan angle.

7 IMPLEMENTATION

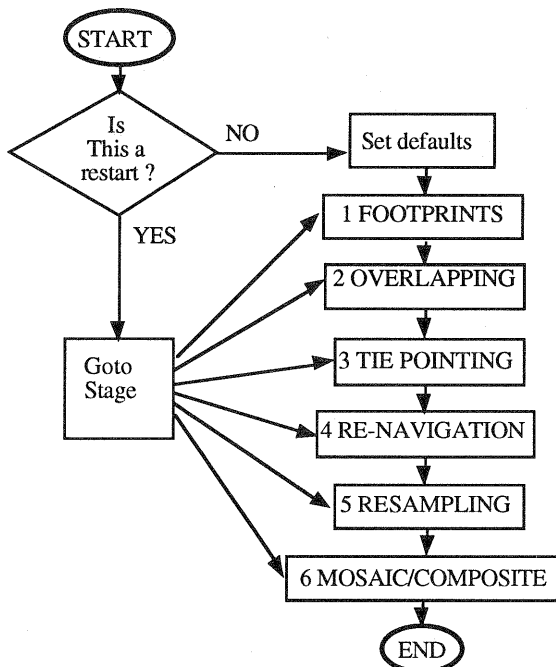


Figure 2. Flow diagram of the UCL MOSAIC system showing capability to restart from any stage in the process.

This section gives a brief description of the implementation and the data flow of the UCL mosaicing system. The system consists of many programs written in C, the Unix C shell command language (csh) and ported subroutines from APOLLO

and JPL's VICAR system. All the ported code was originally written in FORTRAN. C-Shell scripts were written to call all required programmes and to keep track of the processing stages. Organisation of the MOSAIC system is illustrated in figure 2.

All frame location and frame corner coordinate information is stored in a default file so that it can be used to restart mosaic processing at intermediate stages for whatever reason. There are six different stages at which the process can be restarted as illustrated in the flow chart. The program Overlap scans through the frame corner coordinates file and creates the overlap file. The Overlap file is a text file and has two fields per line: frame no. of left image, frame no. of right image. This is used in the tie pointing process to identify overlapping pairs. Footprint is a display program and displays all overlapping images in the output space as rectangles using the frame corner coordinates file. This can be used to ensure that the selected input images give full coverage of the area of interest Figure 3. shows a schematic diagram of the data flow for AVHRR.

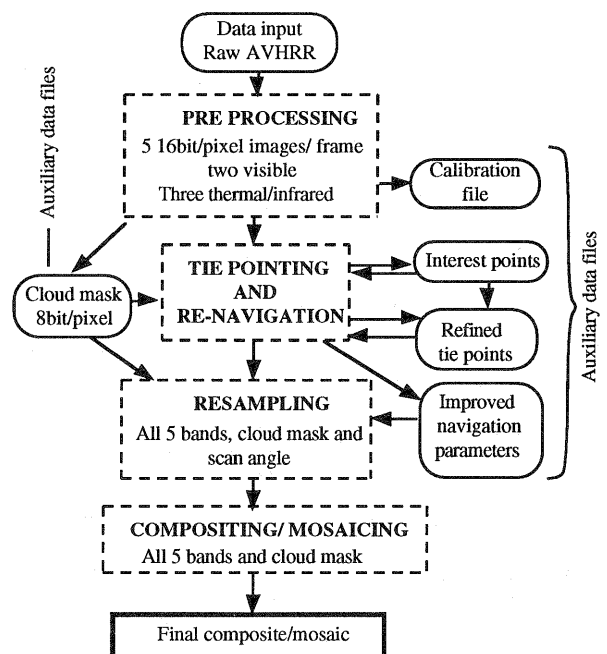


Figure 3 Schematic diagram of the data flow showing files created at each stage.

8 RESULTS AND ERROR ANALYSIS

This section shows mosaics produced from raw AVHRR and LANDSAT-TM SOM and presents a preliminary analysis of the ground errors. The AVHRR is a five channel imaging sensor designed primarily for meteorological applications (Kidwell 1988[11]). At a nominal orbit altitude of approximately 850 kilometres, with a swath width of 2800km of 2048 pixels stretching to 55.4 degrees either side of nadir it has a ground instantaneous field of view (IFOV) of approximately 1.1x1.1km at nadir which increases to 4x6km (along track x across track) at the extreme edge of the swath. The very wide swath of AVHRR means that solar zenith angle, and hence pixel incident irradiance, varies greatly across the swath. This effect can be reduced by normalising the pixel radiances, in the solar reflective channels to the equivalent of an overhead Sun. This correction takes no account of the true surface orientation or BRDF. Another effect which is worsened by the extreme viewing angles of the AVHRR swath is atmospheric scattering of radiance directly to the sensor. Currently no correction for this has been implemented because it requires knowledge of the atmospheric optical depth and because the larger ground IFOV makes wide-angle pixels less useful for mosaic production. Given these provisos, tie-points have been automatically generated for a number of different combinations of AVHRR scenes in the Aral Sea Rondonia and LANDSAT-TM in Kuwait areas. The resulting co-located images have been composited

with some operator intervention in cloud masking and radiometric adjustments for blending purposes. In the case of the Rondonia and Aral Sea images the same task has been performed for images from different years so that the time sequence cross-fading between these can be used to demonstrate temporal change without registration problems. The relative and absolute accuracy of the resampled image results have been estimated by comparing the output coordinates of manually selected points between scenes and by comparison of those coordinates with measured latitude/longitude values from ONC (1:1000000 scale) charts. A mosaic of pre-geocoded LANDSAT TM images, over Northern Germany, and a description of errors can be found in Newton et al 1992 [19].

8.1 Preprocessing of AVHRR

The input is a list of potential contributing images (frames) for the mosaic. For each frame the visible and near IR channels (1 and 2) were calibrated to normalised exoatmospheric reflectance and solar zenith angle adjusted to correct for a Lambertian surface. The thermal channels (4 and 5) were calibrated to brightness temperature and used to create a cloud mask. The cloud masks were dilated by +3 pixels to reduce cloud edge and cloud shadow contamination and then employed as masks for the interest point generation. Figure 5 shows the importance of the cloud mask to generate reliable interest points. Figure 4 gives the processing parameters for results shown here.

8.2 Tie point culling

Tie points are computed on a pairwise basis and re-navigation is performed for the whole mosaic simultaneously. Therefore results for a pair of images are more easily presented. Figure 6 shows the distribution of the interest points, potential tie point

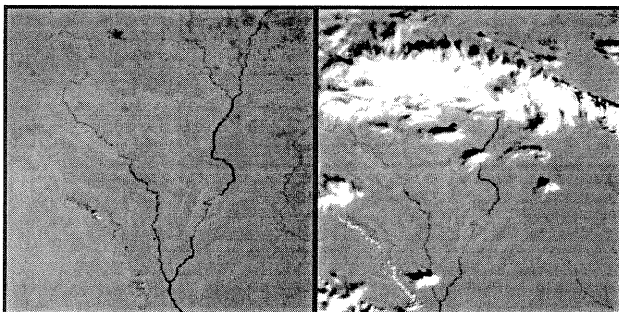
conjugates and final tie points as a function of swath position. The histograms were generated by dividing the image into 16 pixel wide along-track strips and summing the number of points in each strips. This count is plotted against the strip number (column number) to obtain the histogram in Figure 6.

Image Name	Image 1	Image 2
Image Date	24/07/84	17/08/84
Cloud Masking Thresholds/K	294.4	289.0
Number of Interest Points	885 *1800	789 *1800
Number of Potential Tie-Points pairs	9975 *12987	
Number of Tie-Points after ALSC & Locality and Singularity tests	197 *387	
Final Tie-Points After Quadratic Surface fit	49 *25	
Number of Iterations in Surface fit	3 *5	

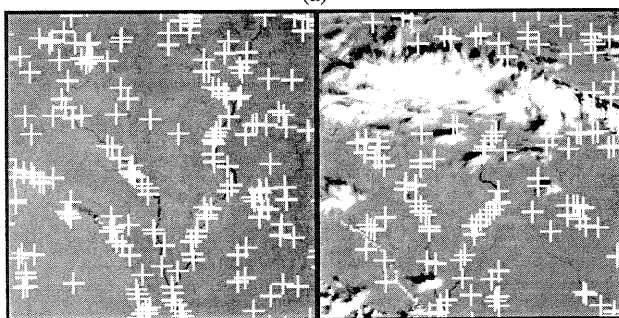
Parameters Used in the above example

Foerstner Parameters: Tile size - 128x128, Points per Tile - 15, Operation Window - 3x3, Non Maximal Suppression - 9x9
 Disparity Limitation: All points - +/- 0.7 degrees
 ALSC Correlation & Locality and Singularity: Patch radius - 7 pixels, Maximum iterations - 5, Eigenvalue threshold - 50, Window Size - 17x17
 * without cloud mask

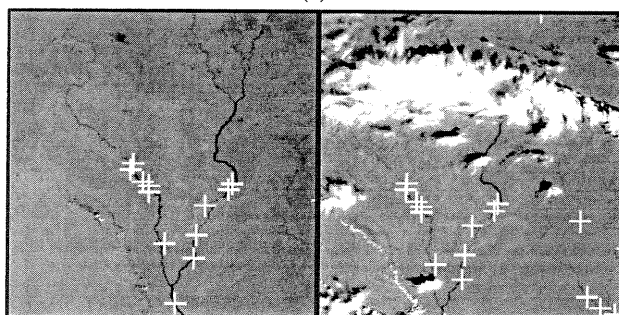
Figure 4 Pre processing and Tie pointing parameters for the example shown in figure 5.



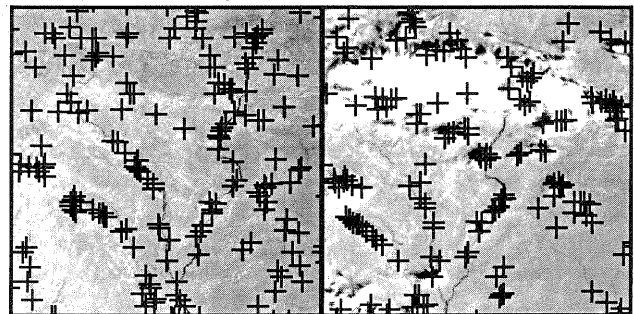
(a)



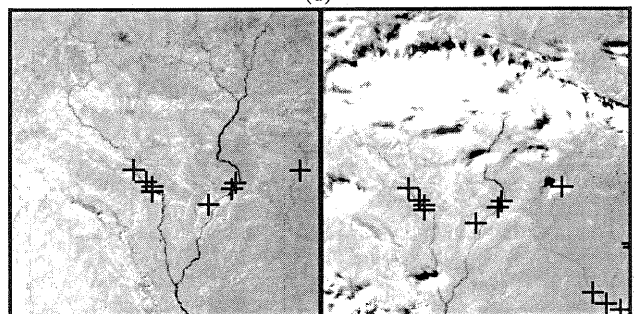
(b)



(c)



(d)



(e)

a. section of the original image (cloud shadows can be seen in the left image section)

left image: Image 1 - 1984/Day 206
 right image: Image 2 - 1984/Day 230.

b. Interest points with cloud mask.

c. Final tie-points with cloud mask.

d. Interest points without cloud mask (points are marked in black for clarity).

e. Final tie-points without cloud mask.

Figure 5 Stages of the Tie-Point generation for Rondonia AVHRR image pair sections, with and without cloud mask.

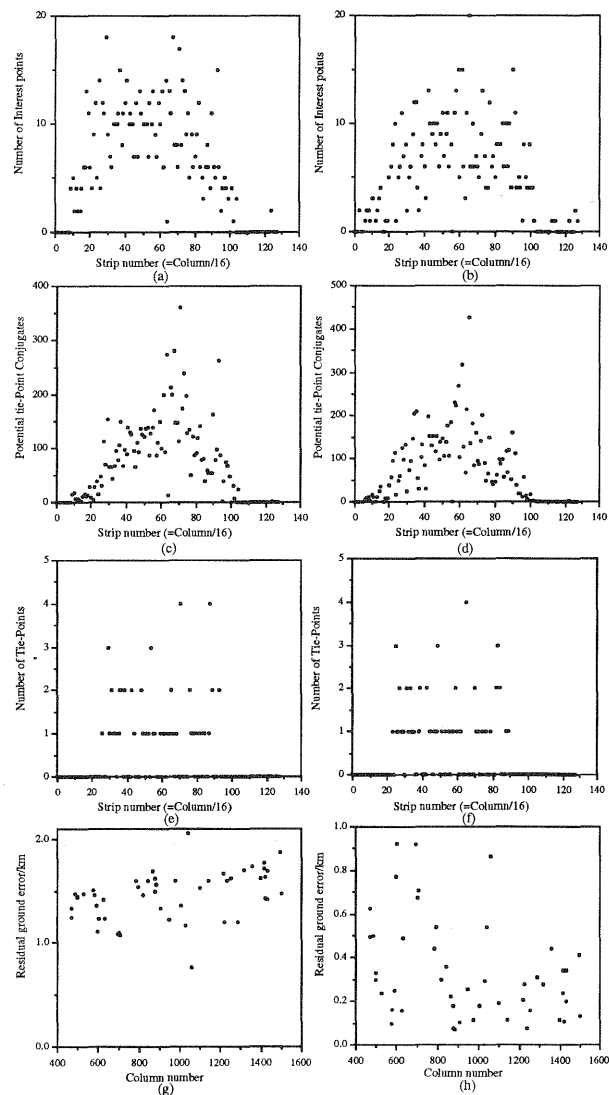
Although the density of the interest points and tie points is a function of the overlap area and cloud mask some idea of the effect of the scan angle can be obtained. From the shape of the histograms (figure 6 c - f) it can be seen that the effect of the scan angle is minimal in the generation of the tie points. Figures 6 g and 6 h shows the ground errors of these tie points, before and after navigation correction, against the column number. It can be seen that there is a larger reduction in error near nadir compared to points away from nadir. This is due to the variation in pixel resolution. The maximum error of this set of tie-points is 0.92km at (604.97, 61.17) (column,row) and minimum error is 0.07km at (885.80,751.62) in image 1. Initial rms error of 1.5km is reduced to 0.4km after navigation correction. Figure 5 (b and c) shows the section of the image pair at the interest point and tie-point stages of this process. Figure 5 d and e shows the effect of the cloud in the tie points generation (interest points and tie points are marked with black crosses for clear visibility). Table 1 shows the data storage required and timings for the AVHRR Rondonia mosaic. Data storage is given for two images and the timings are given for a SUN SPARC station 2 with a local 1GB disk.

Processing Stage	Data Space required	Timing
Pre Processing	40MB	45min/frame
Tie pointing Interest points generation and Tie points	<1MB	45min/pair
Global Re-Navigation	<1MB	15min/pair
Resampling out put: All 5 bands, Scan Angle and Cloud mask	107MB	140min/frame
Mosaicing	107MB	10min/band

Table 1. Data space and timings for the AVHRR Rondonia example show in figure 5 with cloud masking. Timing given is for a SUN SPARC station 2 with a local 1GB disk space.

8.3 Mosaicing and Blending examples

Figure 7 shows a mosaic of the Aral Sea created from three AVHRR images. Images used for this are from three different years (1988,89,91). As the purpose of this mosaic is to study the shrinkage of the Aral Sea over time, mosaicing (as opposed to compositing) was employed to generate the final cloud free mosaic. Figure 7 shows a mosaic of the Aral Sea in 1988. Cloud shadow problems are visible in the mosaic right bottom side of the sea. Table 2 Shows the Absolute and Relative Accuracy assessment for Aral Sea AVHRR images. Table 2 is obtained by comparing the output coordinates of manually selected points between scenes and by comparison of those coordinates with estimated latitude longitude values from ONC charts (scale 1:1000000). Figure 8 shows a mosaic of two LANDSAT-TM SOM images of band 3 of Kuwait. Figure 8a shows the two images without any changes to grey levels. Figure 8b shows a section of the same images after adjusting mean brightness over the overlapping areas. It can be seen that the seam is not visible in areas where there is no change (eg. fires, smoke etc). Figure 8c shows the above area of the mosaic after blending and Figure 8d shows the complete mosaic. Relative accuracy of 9.5m RMS is obtained for the final set of tie-points (312) in this mosaic. The initial RMS error of the tie point data set was 524m.



- Distribution of the Interest points in the Image 1 (Rondonia in 24/7/84).
- Distribution of the Interest points in the Image 2 (Rondonia in 17/8/84).
- Distribution of the Potential tie-points conjugates against image 1 column.
- Distribution of the Potential tie-points conjugates against image 2 column.
- Distribution of the final tie-points against image 1 column.
- Distribution of the final tie-points against image 2 column.
- Distribution of the initial (before navigation correction) residual ground error against image 1 column. RMS error = 1.5km.
- Distribution of the final (after navigation correction) residual ground error against image 1 column. RMS error = 0.4km.

Figure 6. Distribution of the Interest points, potential tie-points, final tie-points and residual error of the tie-points.

Point No. & (lat,lon)	1	2	3	4	5
Image Date	45.825, 62.633	42.617, 58.150	41.217, 61.400	42.283, 59.800	43.300, 60.383
09/08/86	0.536	0.906	0.159	0.639	0.655
18/07/87	0.237	0.923	0.309	0.591	0.582
06/07/88	0.518	0.179	0.701	0.591	0.581
01/08/89	0.518	0.287	0.159	0.429	0.413
17/08/90	0.965	0.179	0.535	0.639	0.723
17/08/91	0.965	0.287	0.159	0.429	0.316
ONC	1.831	1.694	1.850	2.092	2.337

RMS error is in km.

Relative Mean RMS error = 0.5km

Absolute Mean RMS error (ref. to ONC) = 1.9km

Table 2 Absolute and Relative Accuracy assessment for six Aral Sea AVHRR images.

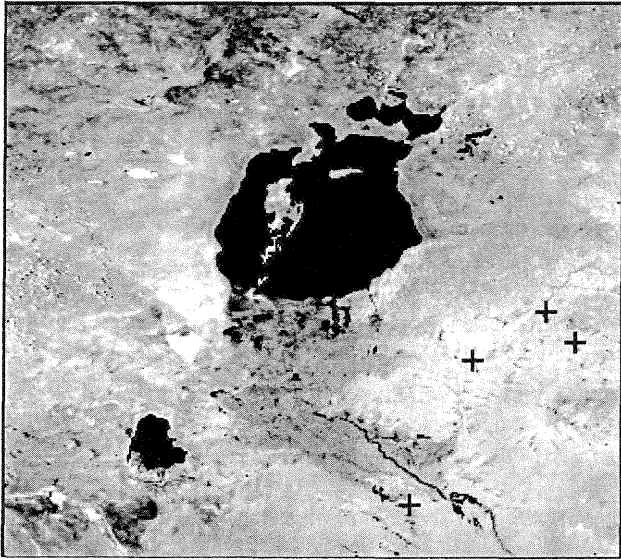


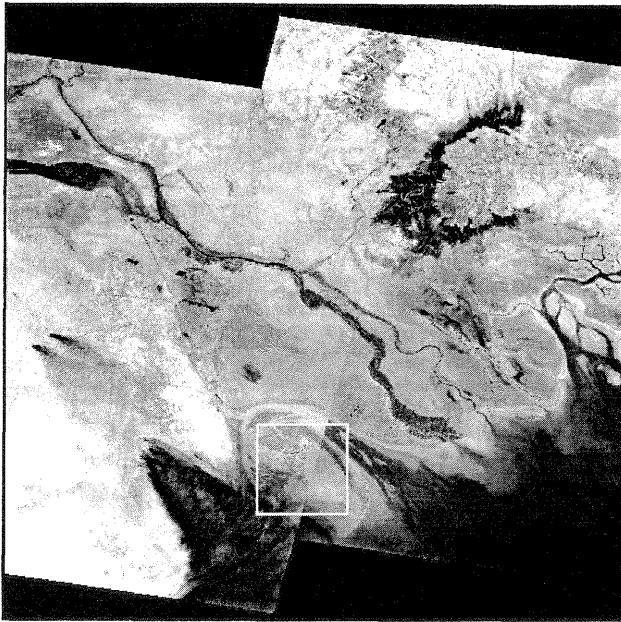
Figure 7 AVHRR channel 2 Aral Sea mosaic image section (date : 18-07-1988). Cloud shadows (marked x) problem is clearly visible in Right bottom of the image.

9 CONCLUSIONS

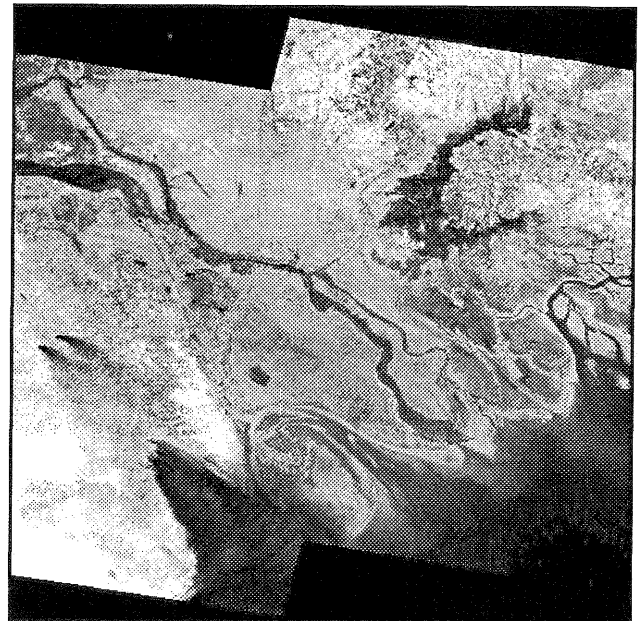
It has been demonstrated that large numbers of high-quality tie-points can be automatically derived using the interest operator plus image correction method described for satellite imagery at two different scales.

Furthermore the tie-points can be used with automated ground error minimisation to improve the relative registration of a large number of overlapping images simultaneously, leading to an improved registration on resampling for all the images. For AVHRR accuracies of 0.4km RMS ground error between tie points and for LANDSAT-TM SOM accuracies of 9.5m RMS ground errors have been achieved.

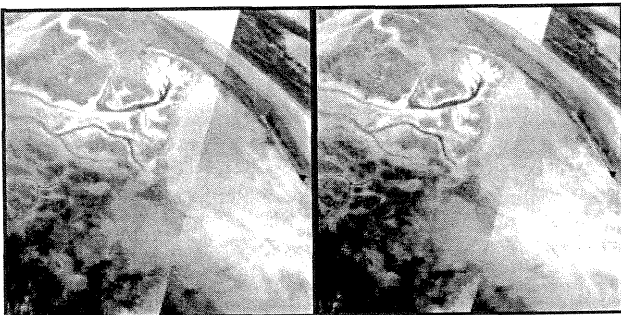
Total mosaic convergence based on pairwise tie-pointing is effective - it is not necessary to identify each tie-point in all the scenes of a given overlap region. The next stage of this process is to produce global image mosaics which can be used in future automated mapping for the NASA Earth Observing System Programme (Muller 1992[18]).



(a)



(d)



(b)

(c)

- a. Images with out any modifications.
 - b. Enlarge section of the overlap area without modification.
 - c. Enlarge section of the overlap area after mean adjustment.
 - d. Images after radiometric blending.
- Left image: Product id - T5311660399105305 date - 22/2/91
 Right image : Product id - T431650399105405 date - 23/2/91
 Band : 3, Map projection : lat lon grid, Grid pitch : 1 sec/pixel

Figure 8 LANDSAT-TM SOM seamless mosaic of Kuwait

ACKNOWLEDGEMENTS

The ALSC operator was implemented at UCL by Paul Otto, Tony Chau, Gillian Peacegood and Mark Upton. Jamal Zemerly implemented the Foerstner operator and previous work on automation of tie-point generation under this scheme has been performed by David Allison. The APOLLO AVHRR processing system was provided, for media cost only, in its VMS/Fortran form by Roger Saunders of the UK Meteorological Office. Nevin Bryant supplied a copy of the Jet Propulsion Laboratories planetary image mosaicing system. LANDSAT-TM data are copyright EOSAT. AVHRR data of Rondonia was supplied by Compton Tucker of NASA/GSFC and of the Aral Sea area by NOAA/NESDIS. This work was supported by the Erd-sicht exhibition of the Kunst-und Ausstellungshalle der Bundesrepublik Deutschland, Bonn and the UK Natural Environment Research Council under grant number GR3/7902.

REFERENCES

- [1] Allison, D. and Muller J-P. 1992. An Automated System for Sub-Pixel Correction and Geocoding of Multi-Spectral and Multi-Look Aerial Imagery - Proceedings XVII ISPRS Congress, Washington D.C..
- [2] Allison D., Zemerley M.J.A. and Muller J-P. 1991. Automatic Seed Point Generation for Stereo Matching and Multi-image Registration IGARSS 1991, Volume IV, Proc. IGARSS Symposium, Espoo, Finland: 2417-2421.
- [3] Barnsley M. and Muller J-P . 1991. Measurement, Simulation and Analysis of the Directional Reflectance properties of Earth Surface Materials ESA SP-319, Proc. 5th Int. Coll. Physical Measurements and Signatures, Courcheville, France: 375-382.
- [4] Barragy E J and Evans K F. 1988. Automated Mosaicking of Planetary Imagery: the VICAR/IBIS Approach, Rev.1 Jet Propulsion Laboratory, California Inst. of Tech., Image Processing Applications Development Section.
- [5] Duggin M. J., Piwinski D., Whitehead V. and Ryland G. 1982. Scan Angle Dependence of radiance recorded by the NOAA-AVHRR Proceedings of SPIE, Advanced Remote Sensing, San Diego, California, August 1982.
- [6] Foerstner W. 1986. A Feature Based Correspondence Algorithm for Image Matching Int. Arch. of Photogrammetry and Remote Sensing, 26(3): 150-166.
- [7] Foerstner W and Gulch E. 1987. A Fast Operator for Detection and Precise Location of Distinct Points, Corners and Centres of Circular Features ISPRS Inter-Commission Workshop, Interlaker, June 1987, pp. 281-305.
- [8] Gallaudet T C and Simpson J J. 1991. Automated Cloud Screening of AVHRR Imagery Using Split-and-Merge Clustering Remote Sensing of the Environment, 38: 77-121.
- [9] Gruen A W. 1985. Adaptive Least Squares Correlation: a powerful image matching technique S. Afr. J. of Photogramm., Rem. Sens. and Cart., 14(3): 175-187.
- [10] Holben B. 1986. Characteristics of Maximum Value Compositing Images from Temporal AVHRR Data Int. J. of Rem. Sens., 7: 1417-1434.
- [11] Kidwell K.B. 1990. Global Vegetation Index User's Guide. NOAA/NESDIS, National Climatic Data Center, Washington D.C..
- [12] Muller J-P. 1989. The GENESIS Project: automated satellite image understanding systems In Keynote Address to the 15th Ann. Conf. of the Remote Sensing Soc., Bristol UK, pp 9-14.
- [13] Muller J-P. and Eales P. 1990. Global Topography Accuracy Requirements for EOS. IGARSS 1990, Proc. IGARSS Symposium, Washington,DC..
- [14] Muller J-P., Allison D., Cook A.C., Day T., Eales P., Holden M., Iliffe J.C., Mandanayake A., Newton A., Tildsley K. and Zemerly J. 1992. Global Mapping of Earth and Mars using Automated Image Understanding Techniques on Remotely-sensed data. Earth and Space Science Information Systems, (Abstract only), Pasadena, CA 10-13 Feb.
- [15] Muller J-P. and Schreier G. 1992. The Global change Video - New Media to demonstrate Global Change Remote Sensing Data Animations. EUR-ISKY 1992, Proc. European ISY Conference, (Abstract only) Munich, Germany.
- [16] Muller J-P., Cook A.C., Day T. and Iliffe J.C. 1992. Global topography of Mars from Automated Image Understanding of Viking Orbiter data. Proceedings IV/6 ISPRS Congress, Washington D.C..
- [17] Muller J-P., Day T., Eales P., Johnston R., Kelly K., Mandanayake A., Newton A., Rees D., Richard S., Rhoads G., and Tildsley K. 1992. Towards Photo-Realistic Visualisation of Global Change Phenomena using Image Understanding of Remotely Sensed Data. IEEE Computer Graphics and Applications (submitted).
- [18] Muller J-P. 1992 Global Mapping Products for the NASA Earth Observing System Programme. Invited paper. Special Session 4. Aug. 1992, ISPRS Congress, Washington D.C..
- [19] Newton A., Mandanayake A., Tildsley K. and Muller J-P. 1992. Satellite Image Mosaics form Automatic Scene Re-navigating. Satellite Symposium Number 2, Image Processing, GIS and Space-Assisted Mapping, at the European International Space Year Conference, Munich, Germany.
- [20] Otto G.P. and Chau T.K.W. 1989. Region Growing Algorithm for Matching of Terrain Images. Proc. of 4th Alvey Vision Conference, and Image and Vision Computing, Image and Vision Comp. 7(2):83-94.
- [21] Saunders R.W. 1988. The Determination of Broad Band Surface Albedo from AVHRR Visible and Near-Infrared Radiances. International Journal of Remote Sensing, 9:1491-1502.
- [22] Saunders R.W. and Kriebel K. 1988. An Improved Method for Detecting Clear Sky and Cloudy Radiances from AVHRR data, Int. J. Rem. Sens. 9:123-150.
- [23] Saunders R.W. and Kriebel K. T. 1988. Errata Re: An Improved Method for Detecting Clear Sky and Cloudy Radiances from AVHRR data, nt. J. Rem. Sens. 9:123-150. International Journal of remote sensing, 9:1393-1394.
- [24] Saunders R.W. and Pescod R.W. 1988. A User Guide to the APOLLO scheme on HERMES/HOMER. Meteorological Office Internal Report, Met.O. 19, Branch Memo 87.
- [25] Simpson J.J. and Humphrey C. 1990. An Automated Cloud Screening Algorithm for Daytime AVHRR Imagery. J. GeoPhys. Res., 95, Number C8, August 15th: 13459-13482.
- [26] Slama C.C. 1980. Manual of Photogrammetry. Fourth Edition, American Society of Photogrammetry, Va 22046, Chapter 9.